ELSEVIER

Normal oscillatory modes of rotating orthotropic disks

Atefeh Khoshnood, Mir Abbas Jalali*

*Center of Excellence in Design, Robotics and Automation, Department of Mechanical Engineering,
Sharif University of Technology, Azadi Avenue, Tehran, Iran*

Abstract

We present the governing equations of transverse vibrations for rotating cylindrically orthotropic disks and calculate their normal oscillatory modes. We use a collocation method to discretize the ordinary differential equation that determines the radial variation of the lateral displacement field in the linear regime. We then construct a nonlinear eigenvalue problem in the matrix form for given azimuthal wavenumbers and compute the eigenfrequencies and their conjugate mode shapes through solving a determinantal equation followed by evaluating the adjoint matrix of a singular linear map. We reveal some notable features of mode shapes in isotropic and orthotropic rotating disks and discuss on their eigenfrequency spectra as the material and geometric properties are varied.
© 2008 Elsevier Ltd. All rights reserved.

1. Introduction

Rotating disks are major components of hard disk drives in computer technology. They are accessed by magnetic heads that are capable of recording (reading) the data on (from) the magnetic material, which is usually protected by a nano-scale layer of hydrogenated amorphous carbon. There is an air gap between the head and the disk whose major function is to levitate the head through aerodynamic forces and prevent the direct contact between the head and the disk. The air gap, however, must be small enough to permit the leaked magnetic field (of the head) to pass through the carbon coat and reach the magnetic material. This requirement puts severe constraints on the vibration characteristics of the disk. Moreover, data access rate is directly proportional to the rotational speed of the disk, which cannot be increased endlessly due to subsequent emergence of stochastic oscillations near resonant speeds. Recent studies of Jalali and Angoshtari [1], and Angoshtari and Jalali [2] based on projected Nowinski's [3,4] governing equations showed that chaos is an inherent characteristic of spinning disks that occurs in long time scales. Detection and control of chaotic response to the harmonically exerted aerodynamic force is still an unresolved technological problem.

The fundamental step in the study of full nonlinear equations is to unveil the natural frequencies and mode shapes (i.e., the eigenmodes) of spinning disks in the linear regime. This very first step, however, is so difficult to allow for exact analytical treatment of the problem. The power series solutions of the rotating disk problem

---

*Corresponding author. Tel.: +98 21 6616 5688.

E-mail addresses: atefeh_khoshnood@mech.sharif.edu (A. Khoshnood), mjalali@sharif.edu (M.A. Jalali).

(in the Nowinski theory for isotropic plates) were constructed by Everesman and Dodson [5]. Soon after their approximate method, a numerical method was developed by Barasch and Chen [6] who assumed a linear combination of four independent solutions and integrated the governing equations of radial eigenfunctions using Adam's method and obtained a determinantal equation for finding the eigenfrequencies. Their method gives more accurate results than series solutions [7], but its implementation is costly because at each step one needs to guess an eigenvalue and integrate a system of ordinary differential equations (ODEs) over the radial domain, and then check for the fulfillment of the frequency equation. Therefore, the integration phase must be repeated until the eigenvalue converges. More recently, Bauer and Eidel [8] applied the Ritz–Galerkin [15] method and constructed an infinite dimensional eigenvalue problem for computing the natural frequencies of isotropic Nowinski disks in the linear regime. They found the solutions of an auxiliary truncated problem and used them as a basis set for expanding the transverse displacement field of a rotating disk in the radial direction. Although Bauer and Eidel's [8] method is analytical, the need for the evaluation of weighted integrals (while applying the Ritz–Galerkin method) slows down the calculation procedure of normal modes and complicates their subsequent applications in nonlinear theories.

Increasing demand for manufacturing high speed and light rotating disks, motivated us to think of cylindrically orthotropic composites as candidates for future substitutes of the main material of the hard disk core, which carries dynamical loads and supports the magnetic material and its protective coating. Among other industrial applications of orthotropic composites one may quote extremely high-speed energy storage flywheels, gas turbine components and new generations of light momentum wheels used as spacecraft and satellite attitude controllers. Many authors have already investigated the stress field and its singularities (see Ref. [9] and references therein), and buckling of rotating orthotropic disks [10]. It was only recently that natural frequencies of such systems were calculated using finite element methods [11–13] and a layer-wise theory [14]. These strategies, however, are not favored if one continues the computations in the nonlinear regime or requires fast and accurate decomposition of bending waves for control purposes. Moreover, mode shapes of rotating orthotropic disks and the effects of material and geometrical parameters on them, are other central issues yet to be explored precisely.

In this paper, we attempt to calculate the eigenmodes of rotating, cylindrically orthotropic disks using an efficient numerical method. Our method is based on the direct collocation of the ODE that determines the radial dependence of transverse displacement field. Boundary conditions of any type can be easily imposed in our method and mode shapes are calculated at the same time that the eigenfrequencies are found. In Section 2 we use Nowinski's [3] fundamental assumptions and derive the governing equations of transverse vibrations in rotating orthotropic disks and linearize them in Section 3. We then assume a harmonic response and expand the transverse displacement component in Fourier series of the azimuthal angle, and derive an ODE for the radial eigenfunctions. We collect the radial eigenfunctions and their derivatives in a state vector and discretize the governing ODE of this state vector using a collocation scheme in Section 4. We then derive a system of linear equations for the state variables at grid points and obtain a nonlinear eigenvalue problem whose eigenvectors determine the shape of oscillatory modes. We present some examples in Section 5 and investigate the modal properties of rotating disks by varying some important parameters of the disk. We conclude the paper by highlighting the advantages of using composite materials in hard disk drives.

2. Governing equations of motion

We consider a thin, cylindrically orthotropic, annular plate of uniform thickness h that rotates with the constant angular velocity Ω. The outer and inner radii of the disk are b and a, respectively. The disk has a free outer edge and its inner edge is clamped to a rigid hub. To represent the governing equations and their corresponding boundary conditions, we adopt the usual polar coordinates (r, θ, z). The origin of the coordinate system is the intersection point of the axis of rotation and neutral plane of the disk. The z-axis coincides with the rotation axis and it is normal to the undeformed neutral plane of the disk. Nowinski's theory begins with von Karman's assumption that the displacement field

$$u_r = u_r^\circ(r, \theta, t) - zw_{,r}, \quad u_\theta = u_\theta^\circ(r, \theta, t) - zr^{-1}w_{,\theta}, \tag{1}$$

at an arbitrary point inside the medium, varies linearly along the plate thickness. Here $(u_r^\circ, u_\theta^\circ)$ is the vector of in-plane displacements (in the radial and azimuthal directions), and $w = u_z(r, \theta, t)$ is the displacement of the neutral plane of the disk in the transversal z-direction. The operator $(\ )_{,\mu}$ denotes a partial derivative with respect to μ. From Eq. (1) one can compute the strain components ε_r, ε_θ and $\varepsilon_{r\theta}$ (Eqs. (3)–(10) in Ref. [16]), which are related to the stress components through the constitutive equations of a cylindrically orthotropic material (Eqs. (6)–(18) in Ref. [16]):

$$\sigma_r = \frac{E_r}{1 - v_{r\theta}v_{\theta r}}(\varepsilon_r + v_{\theta r}\varepsilon_\theta), \tag{2}$$

$$\sigma_\theta = \frac{E_\theta}{1 - v_{r\theta}v_{\theta r}}(\varepsilon_\theta + v_{r\theta}\varepsilon_r), \tag{3}$$

$$\sigma_{r\theta} = G_{r\theta}\varepsilon_{r\theta}, \tag{4}$$

$$\frac{E_\theta}{E_r} = \frac{v_{\theta r}}{v_{r\theta}}. \tag{5}$$

Here E_r and E_θ are, respectively, Young's moduli in the radial and azimuthal directions, $v_{r\theta}$ and $v_{\theta r}$ are Poisson's ratios, and $G_{r\theta}$ is the shear modulus. The resultant normal and shear forces are thus calculated as

$$(N_r, N_\theta, N_{r\theta}) = \int_{-h/2}^{+h/2}(\sigma_r, \sigma_\theta, \sigma_{r\theta})\,\mathrm{d}z. \tag{6}$$

Let us introduce the stress function F so that

$$N_r = r^{-1}hF_{,r} + r^{-2}hF_{,\theta\theta} - \tfrac{1}{2}\rho h\Omega^2 r^2, \tag{7}$$

$$N_\theta = hF_{,rr} - \tfrac{1}{2}\rho h\Omega^2 r^2, \tag{8}$$

$$N_{r\theta} = -(r^{-1}hF_{,\theta})_{,r}. \tag{9}$$

The resultant forces defined in Eqs. (7)–(9) satisfy the in-plane equations of momentum balance if we ignore the inertia forces associated with u_r° and u_θ°. This is a basic assumption of Nowinski's theory that guarantees the existence of F. Hamilton's principle and the compatibility equation of strain components lead to the following nonlinear partial differential equations for the evolution of w and the stress function:

$$\rho h w_{,tt} + D_r L_1 w + D_\theta L_2 w + 2D_c L_3 w + \rho h\Omega^2 r w_{,r} + \tfrac{1}{2}\rho h\Omega^2 r^2\nabla^2 w = hL(w, F), \tag{10}$$

$$d_\theta L_1 F + d_r L_2 F + 2d_c L_3 F - (3d_\theta - d_r + v_{r\theta}d_\theta - 3v_{r\theta}d_r)\rho\Omega^2 = -\tfrac{1}{2}L(w, w), \tag{11}$$

where ρ is the mass per unit volume of the disk material, and the operators L_i ($i = 1, 2, 3$) and L are defined as

$$L_1 A = A_{,rrrr} + 2r^{-1}A_{,rrr}, \tag{12}$$

$$L_2 A = r^{-4}A_{,\theta\theta\theta\theta} - r^{-2}A_{,rr} + 2r^{-4}A_{,\theta\theta} + r^{-3}A_{,r}, \tag{13}$$

$$L_3 A = r^{-2}A_{,rr\theta\theta} - r^{-3}A_{,r\theta\theta} + r^{-4}A_{,\theta\theta}, \tag{14}$$

$$L(A, B) = A_{,rr}(r^{-1}B_{,r} + r^{-2}B_{,\theta\theta}) + B_{,rr}(r^{-1}A_{,r} + r^{-2}A_{,\theta\theta}) - 2(r^{-1}A_{,r\theta} - r^{-2}A_{,\theta})(r^{-1}B_{,r\theta} - r^{-2}B_{,\theta}). \tag{15}$$

The constant coefficients in Eqs. (10) and (11) are:

$$D_r = \frac{E_r h^3}{12(1 - v_{r\theta}v_{\theta r})}, \quad D_\theta = \frac{E_\theta h^3}{12(1 - v_{r\theta}v_{\theta r})}, \quad D_{r\theta} = \frac{G_{r\theta}h^3}{12}, \quad D_c = v_{\theta r}D_r + 2D_{r\theta}, \tag{16}$$

$$d_r = \frac{1}{E_r}, \quad d_\theta = \frac{1}{E_\theta}, \quad d_c = \frac{1}{2G_{r\theta}} - \frac{v_{r\theta}}{E_r}. \tag{17}$$

Eqs. (10) and (11) are, respectively, the extensions of Eqs. (6-30) and (6-31) of Ref. [16] to uniformly rotating disks. The associated boundary conditions (see below) that involve the stress function F are also different from the non-rotating case and they affect the solution procedure substantially. We remark that the ignorance of in-plane inertias reduces the number of dependent functions from three to two, and simplifies the governing equations significantly. However, it is justified only for small rotational velocities. For very high-speed disks that the quantities

$$\Omega^2 u_r^{\circ}, \quad \Omega^2 u_{\theta}^{\circ}, \quad 2\Omega u_{r,t}^{\circ}, \quad 2\Omega u_{\theta,t}^{\circ}, \tag{18}$$

cannot be ignored, one should follow a formalism similar to what Baddour and Zu [17,18] developed for isotropic disks.

There are two sets of boundary conditions associated with the governing field equations. The first set of conditions is imposed at the inner radius $r = a$ where the disk is clamped to the central rotating hub. The in-plane displacement fields have zero boundary values at the clamped edge:

$$u_r^{\circ}(a, \theta, t) = 0, \quad u_{\theta}^{\circ}(a, \theta, t) = 0 \tag{19}$$

and the boundary conditions of w are:

$$w(a, \theta, t) = 0, \tag{20}$$

$$w_{,r}(a, \theta, t) = 0. \tag{21}$$

The second set of boundary conditions is imposed at the free edge of the disk, where the bending moment M_r, edge reaction $Q_r + r^{-1}\partial M_{r\theta}/\partial\theta$, and in-plane forces $(N_r, N_{r\theta})$ must vanish (e.g., Eqs. (3)–(15) in Ref. [16]). At $r = b$ we obtain

$$M_r = 0 \Rightarrow w_{,rr} + v_{\theta r}(r^{-1}w_{,r} + r^{-2}w_{,\theta\theta}) = 0, \tag{22}$$

$$Q_r + \frac{1}{r}\frac{\partial M_{r\theta}}{\partial\theta} = 0 \Rightarrow w_{,rrr} + r^{-1}w_{,rr} - k^2 r^{-2}(w_{,r} + r^{-1}w_{,\theta\theta}) + (2\bar{D} - v_{\theta r})r^{-2}(w_{,r\theta\theta} - r^{-1}w_{,\theta\theta}) = 0, \tag{23}$$

$$N_r = 0 \Rightarrow r^{-1}F_{,r} + r^{-2}F_{,\theta\theta} - \frac{1}{2}\rho\Omega^2 r^2 = 0, \tag{24}$$

$$N_{r\theta} = 0 \Rightarrow -r^{-1}F_{,r\theta} + r^{-2}F_{,\theta} = 0, \tag{25}$$

where we have defined $\bar{D} = D_c/D_r$. The boundary conditions (19) cannot be directly used for solving Eq. (11). What we need are the boundary conditions of F at $r = a$. For deriving such conditions we use the relations between the in-plane strain and displacement components:

$$\varepsilon_r^{\circ} = u_{r,r}^{\circ} \equiv \frac{1}{E_{\theta}h}(k^2 N_r - v_{\theta r}N_{\theta}), \tag{26}$$

$$r\varepsilon_{\theta}^{\circ} = u_r^{\circ} + u_{\theta,\theta}^{\circ} \equiv \frac{r}{E_{\theta}h}(N_{\theta} - v_{\theta r}N_r), \tag{27}$$

$$\varepsilon_{r\theta}^{\circ} = u_{\theta,r}^{\circ} - r^{-1}u_{\theta}^{\circ} + r^{-1}u_{r,\theta}^{\circ} \equiv \frac{1}{G_{r\theta}h}N_{r\theta}, \tag{28}$$

where we have defined $k^2 = E_{\theta}/E_r$ and used the constraint $v_{r\theta}E_{\theta} = v_{\theta r}E_r$ (see Eqs. (2)–(5)) to get $v_{r\theta} = v_{\theta r}/k^2$. Since $u_{\theta,\theta}^{\circ}$ and u_r° vanish at the clamped edge, from Eq. (27) we obtain

$$F_{,rr} - v_{\theta r}(r^{-1}F_{,r} + r^{-2}F_{,\theta\theta}) + \tfrac{1}{2}(v_{\theta r} - 1)\rho\Omega^2 r^2 = 0 \quad \text{at } r = a. \tag{29}$$

We now differentiate Eqs. (27) and (28) with respect to r and θ, respectively, and eliminate $u_{\theta,r\theta}^{\circ}$ using the resulting equations. This leaves us with the following relation:

$$\varepsilon_{\theta}^{\circ} + r\varepsilon_{\theta,r}^{\circ} - \varepsilon_r^{\circ} - \varepsilon_{r\theta,\theta}^{\circ} = \frac{1}{r}(u_{\theta,\theta}^{\circ} - u_{r,\theta\theta}^{\circ}). \tag{30}$$

Both terms on the right side of Eq. (30) vanish because neither u_r° nor u_θ° depend on θ at $r = a$. Therefore, after substituting from Eqs. (7)–(9) in Eqs. (26)–(28) and then in Eq. (30), we obtain

$$F_{,rrr} + r^{-1}F_{,rr} - k^2 r^{-2}F_{,r} + \left(v_{\theta r} - k^2 - \frac{E_\theta}{G_{r\theta}}\right)r^{-3}F_{,\theta\theta}$$

$$+ \frac{E_\theta}{G_{r\theta}}r^{-2}F_{,r\theta\theta} + \left(v_{\theta r} - \frac{3}{2} + \frac{1}{2}k^2\right)\rho\Omega^2 r = 0 \quad \text{at } r = a. \tag{31}$$

Eqs. (29) and (31) constitute the boundary conditions of F at the inner clamped edge. For an isotropic material we have $v_{r\theta} = v_{\theta r} = v$, $E_\theta = E_r = E$ and $G_{r\theta} = E/[2(1 + v)]$. One can readily verify that with the assumption of isotropy, our governing equations (10) and (11) and their associated boundary conditions result in Eqs. (1)–(11) of Ref. [7].

3. Linearized equations

The solution of Eq. (11) consists of a linear part F_l and a nonlinear part F_n that satisfy the following relations:

$$d_\theta L_1 F_l + d_r L_2 F_l + 2d_c L_3 F_l = (3d_\theta - d_r + v_{\theta r}d_\theta - 3v_{r\theta}d_r)\rho\Omega^2, \tag{32}$$

$$d_\theta L_1 F_n + d_r L_2 F_n + 2d_c L_3 F_n = -\tfrac{1}{2}L(w, w). \tag{33}$$

Consequently, the term $L(w, F)$ in Eq. (10) becomes $L(w, F) = L(w, F_l) + L(w, F_n)$. It is remarked that Eq. (32) is identical to Eq. (7) of Ref. [9]. Since we are interested in the normal modes of linear oscillations, we ignore the nonlinear terms $L(w, w)$ and $L(w, F_n)$ in our subsequent analysis and investigate the solutions of

$$\rho h w_{,tt} + D_r L_1 w + D_\theta L_2 w + 2D_c L_3 w + \rho h\Omega^2 r w_{,r} + \tfrac{1}{2}\rho h\Omega^2 r^2\nabla^2 w = hL(w, F_l). \tag{34}$$

The governing equation of F_l is independent of w and its boundary values at the inner and outer edges have no θ dependence. Thus, the homogeneous and particular solutions of F_l will depend only on r. Defining $\alpha = a/b$, Eqs. (32), (24), (29) and (31) result in (see also Eq. (8) in Ref. [9])

$$F_l = \rho\Omega^2[c_1 a^{3-\sqrt{k}}r^{1+\sqrt{k}} + c_2 a^{3+\sqrt{k}}r^{1-\sqrt{k}} + c_3 r^4], \tag{35}$$

where

$$c_1 = \frac{(1-k)[(k^2 - v_{\theta r}^2)\alpha^{3+k} + (k + v_{\theta r})(3 + v_{\theta r})]}{\alpha^2(9 - k^2)(1 - k^2)[(k - v_{\theta r})\alpha^{1+k} + (k + v_{\theta r})\alpha^{1-k}]}, \tag{36}$$

$$c_2 = \frac{(1+k)[-(k^2 - v_{\theta r}^2)\alpha^{3-k} + (k - v_{\theta r})(3 + v_{\theta r})]}{\alpha^2(9 - k^2)(1 - k^2)[(k - v_{\theta r})\alpha^{1+k} + (k + v_{\theta r})\alpha^{1-k}]}, \tag{37}$$

$$c_3 = \frac{3 - k^2 - 2v_{\theta r}}{8(9 - k^2)}. \tag{38}$$

In the isotropy limit ($k^2 = 1$ and $v_{\theta r} = v$), F_l becomes [7]

$$F_l = \rho\Omega^2\left[\frac{1}{32}(1 - v)r^4 + c_1 b^2 r^2 + c_2 b^4 \ln r\right], \tag{39}$$

with

$$c_1 = \frac{1}{16}\frac{(1 + v)[3 + v + (1 - v)\alpha^4]}{[1 + v + (1 - v)\alpha^2]},$$
$$c_2 = \frac{1}{8}\frac{\alpha^2(1 - v)[3 + v - (1 + v)\alpha^2]}{[1 + v + (1 - v)\alpha^2]}. \tag{40}$$

The quartic part in Eqs. (35) and (39) is the particular solution of F_l and the other terms are homogeneous solutions.

We seek for the oscillatory solutions of Eq. (34) in the time domain. This suggests to assume $w(r, \theta, t) = W(r, \theta)e^{i\omega t}$ where ω is the frequency of oscillations and $i = \sqrt{-1}$. The continuity of w in the θ-direction implies the periodicity condition $W(r, \theta) = W(r, \theta + 2\pi)$. Therefore, we can expand $W(r, \theta)$ in Fourier series and write

$$w(r, \theta, t) = e^{i\omega t} \sum_{m=-\infty}^{\infty} \psi_m(r)e^{im\theta}. \tag{41}$$

It is the real part of Eq. (41) that gives the physical solution. We define the parameter $\beta^2 = \rho h/D_r$ and introduce the new independent variable $x = r\sqrt{\beta\Omega}$. Substituting Eqs. (41) and (35) in Eq. (34) and collecting the coefficients of $e^{im\theta}$ leaves us with the following ODE for $\psi_m(x)$:

$$\frac{d^4\psi_m}{dx^4} + G_3(x)\frac{d^3\psi_m}{dx^3} + G_2(x)\frac{d^2\psi_m}{dx^2} + G_1(x)\frac{d\psi_m}{dx} + G_0(x)\psi_m = 0, \tag{42}$$

where

$$G_3(x) = \frac{2}{x}, \tag{43}$$

$$G_2(x) = \frac{1}{2}(1 - 8c_3)x^2 - \frac{2m^2\bar{D} + k^2}{x^2} - x_a^2 f_1(x), \tag{44}$$

$$G_1(x) = \frac{3}{2}(1 - 8c_3)x + \frac{2m^2\bar{D} + k^2}{x^3} - \frac{x_a^2}{x}f_2(x), \tag{45}$$

$$G_0(x) = \left(12c_3 - \frac{1}{2}\right)m^2 + \frac{k^2m^4 - 2k^2m^2 - 2\bar{D}m^2}{x^4} + \frac{m^2x_a^2}{x^2}f_2(x) - \lambda^2. \tag{46}$$

Here we have defined $\lambda = \omega/\Omega$, $(x_a, x_b) = (a\sqrt{\beta\Omega}, b\sqrt{\beta\Omega})$, and the functions f_j $(j = 1, 2)$ are

$$f_j(x) = k^{j-1}\left[c_1(1 + k)\left(\frac{x}{x_a}\right)^{k-1} + c_2(-1)^j(k - 1)\left(\frac{x}{x_a}\right)^{-k-1}\right]. \tag{47}$$

Eq. (42) is an ODE with real coefficients. The solution of $\psi_m(x)$ will thus be real. The reason is that Eqs. (10) and (11) involve even–order partial derivatives of $w(r, \theta, t)$ and $F(r, \theta, t)$ with respect to θ and t. The only exception is the last term of the operator $L(A, B)$, but it does not give rise to complex coefficients, for it is a product of two first order partial derivatives with respect to θ. All these mean that circumferential bending waves have not r-dependent phase angles and spiral-like patterns are impossible.

For a non-rotating isotropic disk, Eq. (42) reduces to

$$\frac{d^4\psi_m}{dy^4} + \frac{2}{y}\frac{d^3\psi_m}{dy^3} - \frac{2m^2 + 1}{y^2}\frac{d^2\psi_m}{dy^2} + \frac{2m^2 + 1}{y^3}\frac{d\psi_m}{dy} + \left(\frac{m^4 - 4m^2}{y^4} - \omega^2\right)\psi_m = 0, \tag{48}$$

with $y = \sqrt{\beta}r$. Eq. (48) admits the classical solution

$$\psi_m(y) = A_1 J_m(\sqrt{\omega}y) + A_2 Y_m(\sqrt{\omega}y) + A_3 I_m(\sqrt{\omega}y) + A_4 K_m(\sqrt{\omega}y). \tag{49}$$

J_m and Y_m are the well-known Bessel functions of the first and second kind, and I_m and K_m are modified Bessel functions of the first and second kind, respectively. A_i $(i = 1, 2, 3, 4)$ are constant coefficients. The solution (49) must satisfy the boundary conditions of w. This leads to a system of linear equations

$$\mathbf{B}(m, \omega) \cdot \mathbf{A} = 0, \quad \mathbf{A} = (A_1, A_2, A_3, A_4)^T, \tag{50}$$

with $\mathbf{B}(m, \omega) = [B_{ij}(m, \omega)]$ $(i, j = 1, 2, 3, 4)$ being a 4×4 matrix whose elements consist of Bessel (and modified Bessel) functions and their derivatives at $y_{\min} = a\sqrt{\beta}$ and $y_{\max} = b\sqrt{\beta}$. The frequency equation of a non-rotating disk is thus the simple determinantal equation $\det[\mathbf{B}(\omega)] = 0$, which has infinite number of eigenvalues, each corresponding to an eigenmode. However, the general solution of Eq. (42) and the frequency

equation are not known for rotating disks (neither isotropic nor orthotropic) in terms of elementary and/or special functions. Therefore, we adopt a numerical method for calculating λ and its associated eigenfunction.

4. Direct collocation in the radial direction

Let us introduce the state variables

$$\Phi \equiv (\phi_1, \phi_2, \phi_3, \phi_4)^{\mathrm{T}} = (\psi_m, \psi_m', \psi_m'', \psi_m''')^{\mathrm{T}} \tag{51}$$

and write Eq. (42) in the compact matrix form

$$\frac{\mathrm{d}\Phi}{\mathrm{d}x} = \mathbf{C}(m, \lambda, x) \cdot \Phi. \tag{52}$$

The prime sign denotes the derivative of a function with respect to its argument and the matrix $\mathbf{C}$ is defined as

$$\mathbf{C}(m, \lambda, x) = \begin{bmatrix} 0 & 1 & 0 & 0 \\ 0 & 0 & 1 & 0 \\ 0 & 0 & 0 & 1 \\ -G_0(x) & -G_1(x) & -G_2(x) & -G_3(x) \end{bmatrix}. \tag{53}$$

We now divide the physical x-domain to N intervals of the same length $\Delta x = (x_b - x_a)/N$, and adopt a finite difference scheme [20] to discretize the system of Eq. (52) as

$$\frac{\Phi_{k+1} - \Phi_k}{x_{k+1} - x_k} = \mathbf{C}\left(m, \lambda, \frac{x_{k+1} + x_k}{2}\right) \cdot \left(\frac{\Phi_{k+1} + \Phi_k}{2}\right), \quad k = 1, 2, \ldots, N. \tag{54}$$

Here $\Phi_k = (\phi_k^1, \phi_k^2, \phi_k^3, \phi_k^4)^{\mathrm{T}}$ denotes the state vector at the grid point $x_k = (k-1)\Delta x + x_a$. Defining $\mathbf{I}$ as a 4×4 identity matrix, and after rearrangement of terms in Eq. (54), we arrive at

$$\mathbf{U}_k(m, \lambda) \cdot \Phi_k + \mathbf{V}_k(m, \lambda) \cdot \Phi_{k+1} = 0, \quad k = 1, 2, \ldots, N, \tag{55}$$

where $\mathbf{U}_k(m, \lambda)$ and $\mathbf{V}_k(m, \lambda)$ are square matrices of the form

$$\mathbf{U}_k(m, \lambda) = -\mathbf{I} - \frac{1}{2}\Delta x \mathbf{C}\left(m, \lambda, k\Delta x + x_a - \frac{\Delta x}{2}\right), \tag{56}$$

$$\mathbf{V}_k(m, \lambda) = \mathbf{I} - \frac{1}{2}\Delta x \mathbf{C}\left(m, \lambda, k\Delta x + x_a - \frac{\Delta x}{2}\right). \tag{57}$$

The system of Eq. (55) together with the boundary conditions

$$\phi_1^1 = 0, \tag{58}$$

$$\phi_1^2 = 0, \tag{59}$$

$$\phi_{N+1}^3 + \frac{v_{\theta r}}{x_b}\phi_{N+1}^2 - \frac{v_{\theta r}m^2}{x_b^2}\phi_{N+1}^1 = 0, \tag{60}$$

$$\phi_{N+1}^4 + \frac{1}{x_b}\phi_{N+1}^3 - \frac{1}{x_b^2}[k^2 + m^2(2\bar{D} - v_{\theta r})]\Phi_{N+1}^2 + \frac{m^2}{x_b^3}(k^2 + 2\bar{D} - v_{\theta r})\Phi_{N+1}^1 = 0, \tag{61}$$

constitute a system of $4 \times (N+1)$ equations for $N+1$ unknown vectors Φ_k $(k = 1, \ldots, N+1)$. We assemble all Φ_k in a single vector of dimension $4 \times (N+1)$ as

$$\Psi = (\Phi_1^{\mathrm{T}}, \Phi_2^{\mathrm{T}}, \ldots, \Phi_{N+1}^{\mathrm{T}})^{\mathrm{T}}, \tag{62}$$

and obtain

$$\mathbf{D}(m, \lambda) \cdot \Psi = 0, \tag{63}$$

so that

$$\mathbf{D}(m,\lambda) = \begin{pmatrix} \mathbf{U}_a & \mathbf{0} & \mathbf{0} & \mathbf{0} & \cdots & \mathbf{0} \\ \mathbf{U}_1 & \mathbf{V}_1 & \mathbf{0} & \mathbf{0} & \cdots & \mathbf{0} \\ \mathbf{0} & \mathbf{U}_2 & \mathbf{V}_2 & \mathbf{0} & \cdots & \mathbf{0} \\ \vdots & \vdots & \ddots & \ddots & \ddots & \vdots \\ \mathbf{0} & \mathbf{0} & \cdots & \mathbf{0} & \mathbf{U}_N & \mathbf{V}_N \\ \mathbf{0} & \mathbf{0} & \cdots & \mathbf{0} & \mathbf{0} & \mathbf{V}_b \end{pmatrix}, \tag{64}$$

where $\mathbf{0}$ is a null matrix of dimension 4×4, and the blocks $\mathbf{U}_a$ and $\mathbf{V}_b$ are 2×4 matrices that correspond to the boundary conditions at x_a and x_b [see Eqs. (58)–(61)], respectively. They are:

$$\mathbf{U}_a = \begin{pmatrix} 1 & 0 & 0 & 0 \\ 0 & 1 & 0 & 0 \end{pmatrix}, \tag{65}$$

$$\mathbf{V}_b = \begin{pmatrix} -\dfrac{v_{\theta r} m^2}{x_b^2} & \dfrac{v_{\theta r}}{x_b} & 1 & 0 \\ \dfrac{m^2(k^2 + 2\bar{D} - v_{\theta r})}{x_b^3} & -\dfrac{[k^2 + m^2(2\bar{D} - v_{\theta r})]}{x_b^2} & \dfrac{1}{x_b} & 1 \end{pmatrix}. \tag{66}$$

The linear system (63) has physical solutions for Ψ should the determinant of $\mathbf{D}$ vanish. This gives us the nonlinear eigenvalue equation

$$\det[\mathbf{D}(m,\lambda)] = 0. \tag{67}$$

The roots of Eq. (67) are the eigenvalues of Eq. (42) with the associated boundary conditions at $x = x_a$ and x_b. We denote the eigenvalues by $\lambda_{m,n}$. They are indexed by the azimuthal wavenumber m and the root number $n \geqslant 0$ that indicates the number of the radial nodes of the corresponding eigenvector. We refer to n as the radial wavenumber. Waves with $m > 0$ and $m < 0$ are forward- and backward-traveling, respectively, and ring modes correspond to $m = 0$.

Once the root $\lambda_{m,n}$ is found, we construct the adjoint of $\mathbf{D}(m,\lambda_{m,n})$. Any column of adj$[\mathbf{D}(m,\lambda_{m,n})]$ is thus the eigenvector $\Psi_{m,n}$ associated with $\lambda_{m,n}$ [19] and we have

$$\mathbf{D}(m,\lambda_{m,n}) \cdot \Psi_{m,n} = 0. \tag{68}$$

According to Eqs. (51) and (62), the vector $\Psi_{m,n}$ contains the discretized mode shape $\psi_{m,n}(x_k)$ ($k = 1, 2, \ldots,$ $N + 1$) and its three successive derivatives. This is an interesting result because the derivatives of $\psi_{m,n}(x)$, which can then be used in the calculation of disk slope, bending moments and resultant shear forces, are computed together with the displacement field and with the same accuracy. The vectors $\Psi_{m,n}$ are orthogonal. Consequently, $\psi_{m,n}(x)$ make an orthogonal, complete basis set in the radial direction and the functions $\psi_m(x)$ can be expressed as a linear combination of $\psi_{m,n}(x)$ in the following form:

$$\psi_m(x) = \sum_{n=0}^{\infty} a_{m,n} \psi_{m,n}(x), \tag{69}$$

with $a_{m,n}$ being constant coefficients. They are determined using initial conditions.

An alternative way for the calculation of $\Psi_{m,n}$ is through the method of singular value decomposition (SVD). Application of this method is recommended when a large N is needed to assure the convergence of the eigenvalue equation. Implementation of the SVD technique is quite routine. After computing $\lambda_{m,n}$ one can decompose $\mathbf{D}(m,\lambda_{m,n})$ in the form $\mathbf{D} = \mathbf{E}^{\mathrm{T}} \cdot \mathbf{S} \cdot \mathbf{G}$ [20] where $\mathbf{E}$ and $\mathbf{G}$ are square matrices of the same dimension as $\mathbf{D}$, and $\mathbf{S}$ is a diagonal matrix whose elements are the singular values of $\mathbf{D}$. The column of $\mathbf{G}$ corresponding to the smallest singular value is the eigenvector associated with $\lambda_{m,n}$.

5. Solved examples

To this end, we apply our numerical scheme to explore the normal modes of rotating disks which are clamped to a central rigid hub. Our eigenvalue equation (67) depends on two geometrical parameters: x_a and α, two material properties: $v_{\theta r}$ and k, and the azimuthal wavenumber m. Without loss of generality, we set $x_b = 5$ and vary the ratio α in our analysis. At first, we demonstrate our method for non-rotating and rotating isotropic disks. This helps us to understand the influence of disk rotation on the radial eigenfunctions and probe the accuracy of the collocation scheme. For our isotropic disks we set $v = 0.3$. We then investigate a class of orthotropic disks whose filaments are placed in the hoop direction. This implies $k^2 > 1$. As our case study we choose the graphite–epoxy composite with $k^2 = 40$, $G_{r\theta}/E_r = 0.5$ and $v_{\theta r} = 0.25$.

A preliminary investigation of the eigenvalue equation shows that the function $\det[\mathbf{D}(m, \lambda)]$ is oscillatory (in terms of λ) and its amplitude increases substantially as λ is increased. Therefore, we adopt a hybrid technique to capture all roots of the eigenvalue equation. We first isolate a root by a univariate search, then approach it using the bi-section method. For higher eigenfrequencies, the bi-section method converges to the isolated root so fast because the function $\det[\mathbf{D}(m, \lambda)]$ varies steeply when λ is large. For lower eigenfrequencies a few bi-section steps is followed by Newton's algorithm to speed up the convergency. We start our calculations with $N = 50$ and increase it until the relative accuracy falls below 10^{-6}. For $N = 100$ we have obtained credible results and we do not observe a notable correction on the eigenfrequencies for a larger value of $N = 200$. Table 1 compares the eigenfrequencies computed using the collocation method (given $N = 100$) with the results of analytical equation (50) for a non-rotating isotropic disk with $v = 0.3$ and $\alpha = 0.2$. It is evident that the maximum relative error remains below 0.001, which shows the excellent performance of the collocation method.

Fig. 1 shows the variation of eigenfrequencies versus the parameter α for rotating isotropic (left panels) and orthotropic (right panels) disks. We have plotted $\lambda_{m,n}$ for $0 \leqslant n \leqslant 2$ and $0 \leqslant m \leqslant 3$. As one could anticipate, in both disks the eigenvalues increase as the radial and azimuthal wavenumbers are increased. Disk stiffening is also a natural consequence of increasing the parameter α: all eigenvalues, independent of their radial and azimuthal wavenumbers, are increasing functions of α [7]. Nevertheless, eigenfrequencies of higher azimuthal wavenumbers have a robustness against the variations of α. This robustness is more visible for orthotropic disks whose $\lambda_{m,n}$ curves exhibit a flatness for small values of α as m increases. This property of orthotropic disks is also inherited by their critical buckling load as discussed in Ref. [16] and references therein.

We have analyzed the mode shapes of rotating isotropic and orthotropic disks as the parameter α varies and compared them with mode shapes of classical, non-rotating isotropic disks. Some of our results have been illustrated in Figs. 2 and 3. Our plots display the eigenfunctions $\psi_{m,n}$ for $0 \leqslant n \leqslant 2$ and $0 \leqslant m \leqslant 3$. We have normalized the maximum of each eigenfunction to unity. The eigenfunctions have some anticipated features as far as boundary conditions and radial wavenumbers are concerned: they join the central rigid hub with a zero slope, have a negligible curvature (but not zero) at the outer boundary due to the free edge, and the number of their radial nodes is equal to n.

For a non-rotating isotropic disk with $\alpha = 0.2$ (left panels in Fig. 2) it is seen that radial eigenfunctions have almost the same behavior for different azimuthal wavenumbers m. For the rotating disk of the same $\alpha = 0.2$ (right panels in Fig. 2) differences between mode shapes are more distinguishable. As the azimuthal

Table 1
The eigenfrequencies $\omega_{m,n}$ of a non-rotating isotropic disk computed using analytical and collocation methods for $v = 0.3$ and $\alpha = 0.2$

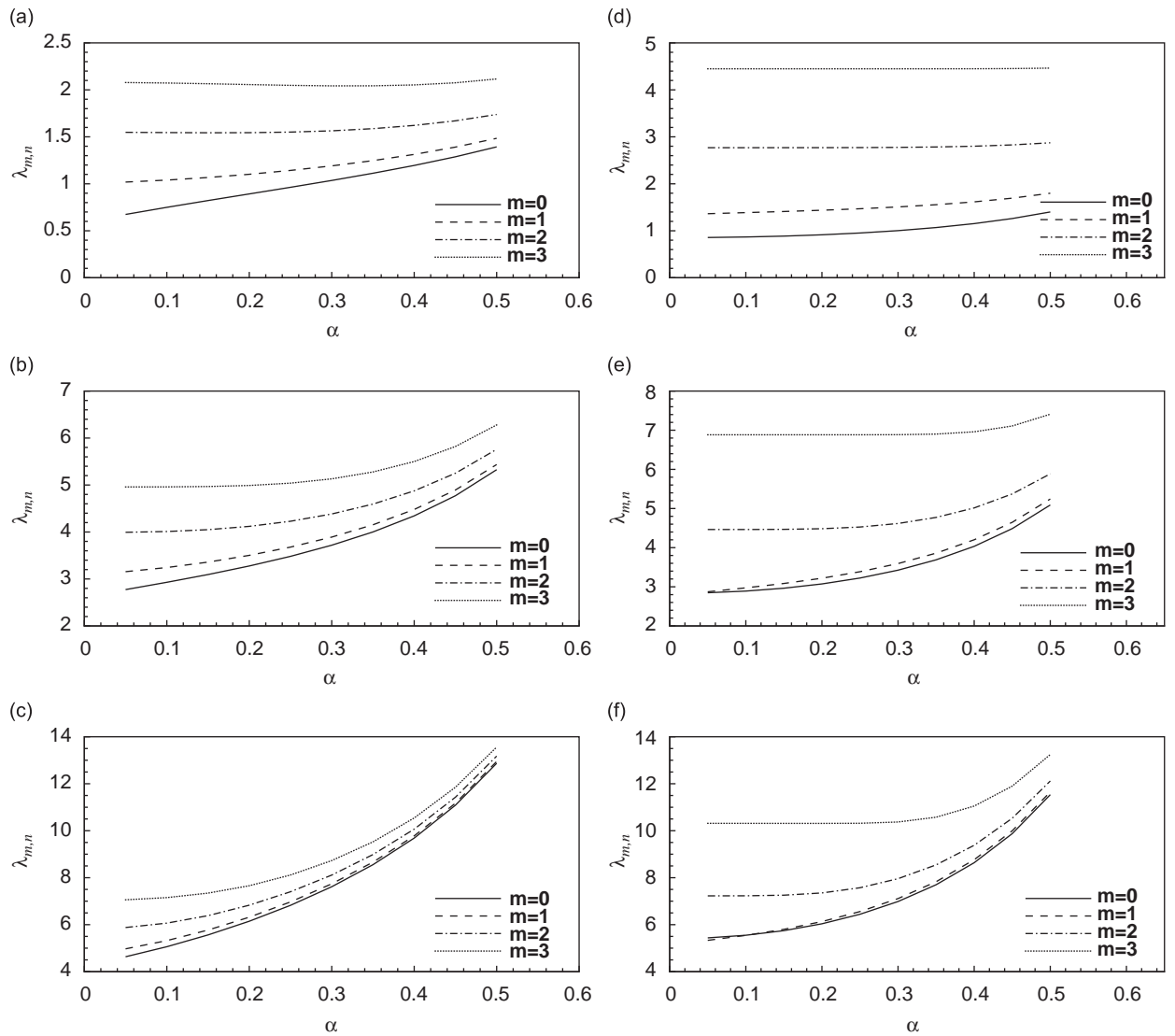| m	Analytical			Collocation ($N = 100$)		
	$n = 0$	$n = 1$	$n = 2$	$n = 0$	$n = 1$	$n = 2$
0	518.109	3229.125	9408.445	518.050	3229.835	9416.601
1	481.303	3452.569	9695.353	481.208	3453.252	9703.452
2	644.710	4195.926	10 612.556	644.625	4196.627	10 620.596
3	1261.468	5541.008	12 261.886	1261.481	5541.982	12 270.250

Fig. 1. Variation of the eigenfrequencies $\lambda_{m,n} = \omega_{m,n}/\Omega$ versus α for $x_b = 5$. Left panels: a rotating isotropic disk with $v = 0.3$. Right panels: a rotating orthotropic disk with $k^2 = 40$, $v_{\theta r} = 0.25$ and $G_{r\theta}/E_r = 0.5$. (a) $n = 0$. (b) $n = 1$. (c) $n = 2$. (d) $n = 0$. (e) $n = 1$. (f) $n = 2$.

wavenumber increases, the local minima/maxima of $\psi_{m,n}$ are shifted to larger radii. The magnitude of such a shift is larger for smaller values of α (left panels in Fig. 3). This property of radial eigenfunctions means that in rotating disks each annular region is dominated by a single azimuthal wave. The physical reason for such a distribution of local extrema is ascribed to the rotation-induced flattening of the disk, which is more effective for large m and in the regions near to the hub. By increasing α, the overall bending stiffness of the disk increases too, and the mode shapes are not affected by the disk rotation considerably. Mode shapes of orthotropic disks (right panels in Fig. 3) show more flattening near the inner edge as m increases. The outward shift of radial nodes is also significant. The trend shows that modes with high azimuthal wavenumbers must be localized near the outer free edge.

The fundamental radial eigenfunctions ($n = 0$) exhibit another interesting feature, which is observed only in rotating disks with small α. That is the negative curvature of $\psi_{0,0}$ and $\psi_{0,1}$ at intermediate radii. We have not identified this feature for waves with $m > 1$. Figs. 2(d), 3(a) and (d) clearly show the transition from a negative to a positive curvature as m increases. We have examined other $k^2 > 1$ values that correspond to
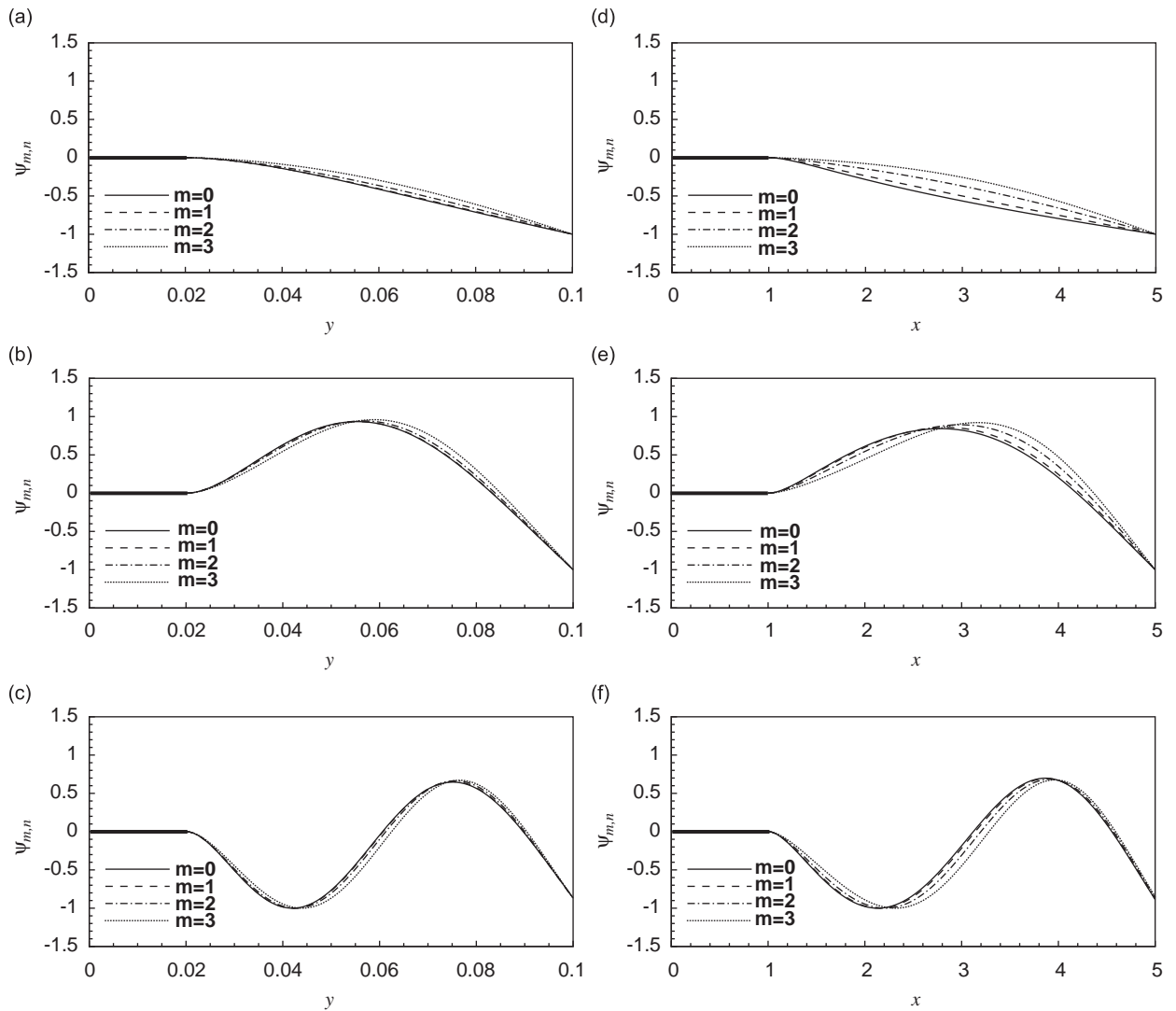
Fig. 2. Radial eigenfunctions of a non-rotating (left panels) and a rotating (right panels) isotropic disk. For both disks we have set $\alpha = 0.2$. The thick solid line shows the rigid central hub, which provides the clamped boundary condition of the disk at its inner edge. (a) $n = 0$. (b) $n = 1$. (c) $n = 2$. (d) $n = 0$. (e) $n = 1$. (f) $n = 2$.

circumferentially reinforced composites. The general behavior of modes is similar to what we reported in Fig. 3. However, mode shapes of radially reinforced composites with $k^2 < 1$ have a different behavior. In Fig. 4 we have demonstrated $\psi_{m,n}$ for an orthotropic disk with $k^2 = 1/40$, $v_{r\theta} = 0.25$ and $\alpha = 0.1$. The material is the same graphite–epoxy composite, but with radially stretched fibers. It is evident that dependency of mode shapes on the azimuthal wavenumber m has become very weak and there is no sign of flattening near the inner boundary for large values of m. This is because the fiber bundles look like radial flexible beams whose interactions with their neighbors in the θ-direction are negligible. In other words, a radially reinforced composite shows little resistance against the propagation of circumferential waves of any wavenumber m.

6. Conclusions

We presented a fast and efficient numerical method based on the direct collocation of a fourth-order ODE to calculate the eigenfrequencies and mode shapes of rotating disks. Our approach is superior to existing methods in the literature because of two reasons. Firstly, the collocation scheme converges very fast by taking
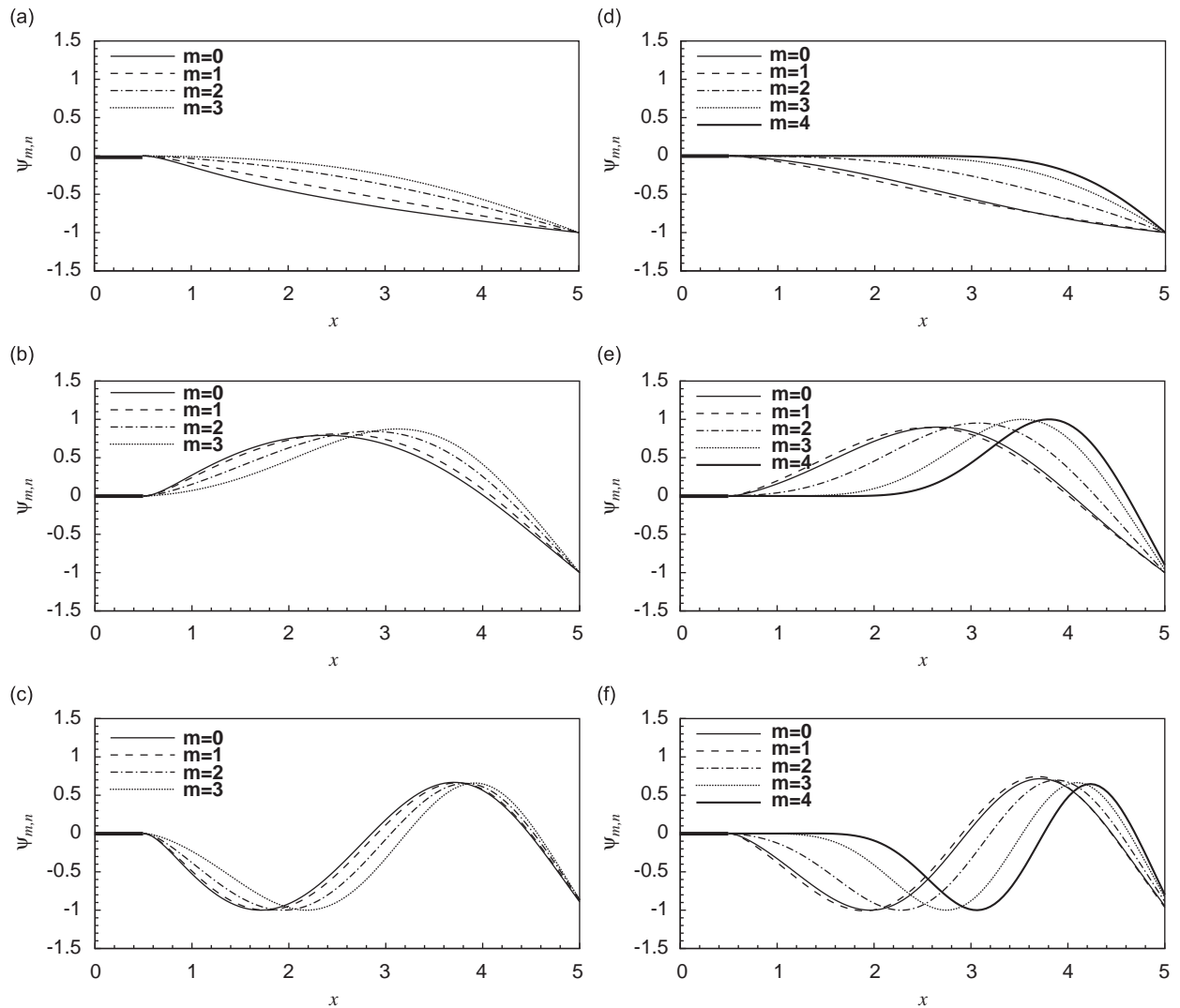
Fig. 3. Same as Fig. 2 but for two rotating disks. Left panels: an isotropic disk with $\alpha = 0.1$ and $v = 0.3$. Right panels: an orthotropic disk with $\alpha = 0.1$, $v_{\theta r} = 0.25$, $G_{r\theta}/E_r = 0.5$ and $k^2 = 40$. (a) $n = 0$. (b) $n = 1$. (c) $n = 2$. (d) $n = 0$. (e) $n = 1$. (f) $n = 2$.

a few hundred grid points for all values of the parameter $0 < \alpha < 1$. Secondly, mode shapes and their derivatives with respect to the radial variable are calculated at the same time that we find the eigenvalues. Moreover, boundary conditions of any type can easily be imposed through the 2×4 matrices $\mathbf{U}_a$ and $\mathbf{V}_b$. The only technical (and time consuming) issue is to isolate the roots of the determinantal equation $\det[\mathbf{D}(m, \lambda)] = 0$. Since $\det[\mathbf{D}(m, \lambda)]$ is an oscillatory function of λ, we suggest to apply the steepest descent method to locate the extrema of $\det[\mathbf{D}(m, \lambda)]$. Noting the fact that a root lies between a maximum and a minimum of $\det[\mathbf{D}(m, \lambda)]$, the classical bi-section algorithm would then provide the most reliable (if not the fastest) route to the isolated eigenfrequency.

Our displays of eigenfunctions for both isotropic and orthotropic disks unveiled a very important property of mode shapes of rotating disks: the extrema of the radial eigenfunctions $\psi_{m,n}$ are shifted to larger radii as the azimuthal wavenumber m increases. This effect is more prominent for orthotropic disks and for small values of the geometrical parameter α. Higher order modes (waves) of orthotropic disks exhibit extreme flattening over a vast region of the disk. The energy of these waves is thus concentrated near the outer edge. We call this phenomenon the *edge localization effect*, which has significant consequences in nonlinear regime when modes begin to interact and stochastic solutions occur in the phase space.
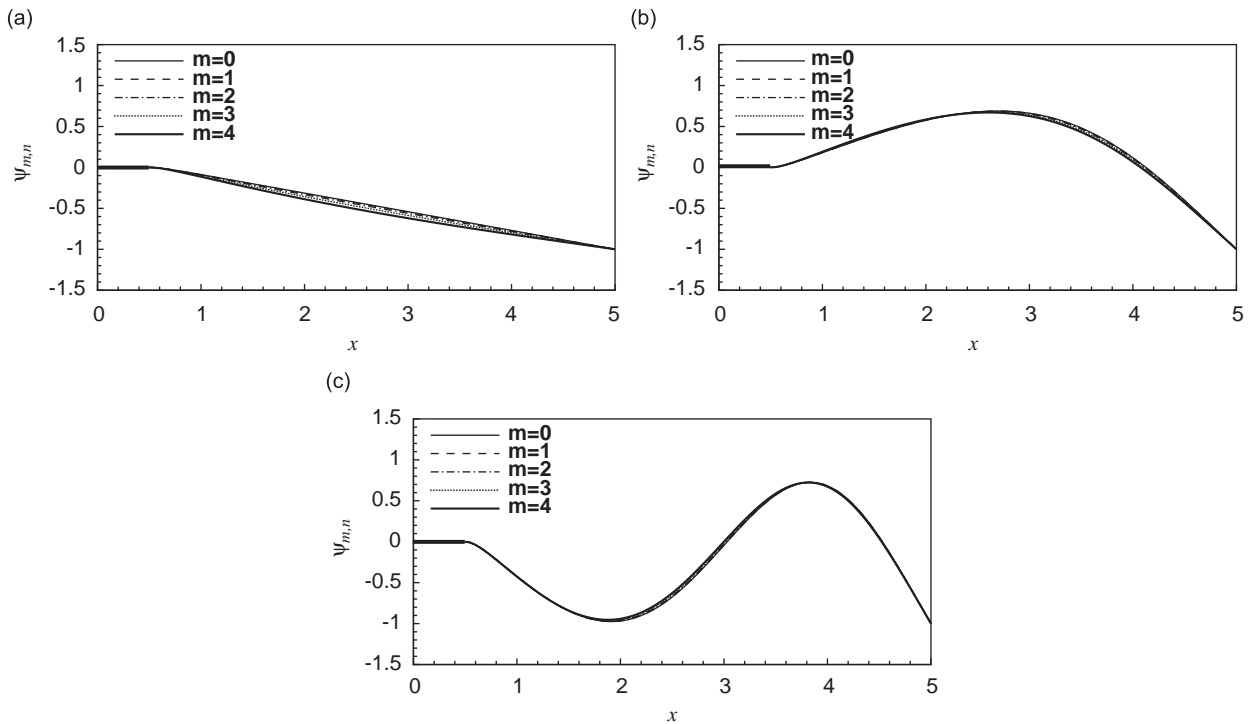
Fig. 4. Radial eigenfunctions of a rotating orthotropic disk with radially stretched fibers for $\alpha = 0.1$. The material properties are $v_{r\theta} = 0.25$, $G_{r\theta}/E_\theta = 0.5$ and $k^2 = 1/40$. (a) $n = 0$. (b) $n = 1$. (c) $n = 2$. It is seen that $\psi_{m,n}$ overlap for different choices of m.

So far, all investigators [1,2,4,7] have studied the interactions of a forward and a backward traveling wave of the same azimuthal wavenumber m under the influence of an external point load of the form $(P_0/r_0)\delta(r - r_0)\delta(\theta - \Omega t)$. The fundamental question that strikes our mind is whether in realistic rotating disks we can excite waves of any azimuthal Fourier number by a prescribed r_0. The answer to this question has become possible by our visualization of mode shapes. As Fig. 3 shows, the extrema (and nodes) of $\psi_{m,n}$ with different azimuthal wavenumbers do not occupy the same annular region. Therefore, we need regionally concentrated initial (or dynamic) loadings to excite a prescribed circumferential wave. For a point load this means that our choice of the pair (m, r_0) is highly constrained. An immediate implication is for the nonlinear development of double-mode circumferential waves, specially for those of the form [1,2,4,7]

$$w(r, \theta, t) = \psi_{m,n}(r)[\xi_n(t)\cos(m\theta) + \eta_n(t)\sin(m\theta)]. \tag{70}$$

Such a wave can be individually treated only if r_0 is chosen in harmony with m. However, in a typical hard disk drive, r_0 is actually time-dependent and the aerodynamic force of the head is indeed a moving point load. Thus, new families of circumferential waves are activated as the head moves in the radial direction. The excited waves (with different m) gradually constitute groups of interacting waves and the disk dynamics enters to a very complex epoch. Identification of regular and stochastic waves in these conditions is a new mathematical challenge, highlighted by the present work. Composite disks with $k^2 < 1$ do not suffer from the mentioned consequences of the distribution of wave components in the radial direction because mode shapes associated with a given radial wavenumber n overlap for all choices of m (see Fig. 4). Radially reinforced composite disks, however, are susceptible to buckling and we do not suggest their application in the hard disk technology.

Acknowledgments

References

[1] M.A. Jalali, A. Angoshtari, Phase space structure of spinning disks, *International Journal of Non-Linear Mechanics* 41 (5) (2006) 726–735.

[2] A. Angoshtari, M.A. Jalali, On the existence of chaotic circumferential waves in spinning disks, *Chaos* 17 (2) (2007) 023120.

[3] J.L. Nowinski, Nonlinear transverse vibration of a spinning disk, *Journal of Applied Mechanics* 31 (1964) 72–78.

[4] A. Raman, C.D. Mote Jr., Non-linear oscillations of circular plates near a critical speed resonance, *International Journal of Non-Linear Mechanics* 34 (1999) 139–157.

[5] W. Eversman, R.O. Dodson, Free vibration of a centrally clamped spinning circular disk, *AIAA Journal* 7 (1969) 2010–2012.

[6] S. Barasch, Y. Chen, On the vibration of a rotating disk, *Journal of Applied Mechanics* 29 (1972) 1143–1144.

[7] A.H. Nayfeh, A. Jilani, P. Manzione, Transverse vibration of a centrally clamped rotating circular disk, *Nonlinear Dynamics* 26 (2001) 163–178.

[8] H.F. Bauer, W. Eidel, Transverse vibration and stability of spinning circular plates of constant thickness and different boundary conditions, *Journal of Sound and Vibration* 300 (2007) 877–895.

[9] R. Jain, K. Ramachandra, K.R.Y. Simha, Singularity in rotating orthotropic discs and shells, *International Journal of Solids and Structures* 37 (2000) 2035–2058.

[10] N. Tutuncu, A. Durdu, Determination of buckling speed for rotating orthotropic disk restrained at outer edge, *AIAA Journal* 36 (1) (1998) 89–93.

[11] D.-S. Liang, H.-J. Wang, L.-W. Chen, Vibration and stability of rotating polar orthotropic annular disks subjected to a stationary concentrated transverse load, *Journal of Sound and Vibration* 250 (5) (2002) 795–811.

[12] K.-N. Koo, Vibration analysis and critical speeds of polar orthotropic annular disks in rotation, *Composite Structures* 76 (2006) 67–72.

[13] Y.-R. Chen, L.-W. Chen, Vibration and stability of rotating polar orthotropic sandwich annular plates with a viscoelastic core layer, *Composite Structures* 78 (2007) 45–57.

[14] M. Tahani, A. Nosier, S.M. Zebarjad, Deformation and stress analysis of circumferentially fiber-reinforced composite disks, *International Journal of Solids and Structures* 42 (2005) 2741–2754.

[15] J.N. Reddy, *Applied Functional Analysis and Variational Methods in Engineering*, McGraw-Hill, New York, 1986.

[16] C.-Y. Chia, *Nonlinear Analysis of Plates*, McGraw-Hill, New York, 1980.

[17] N. Baddour, J.W. Zu, A revisit of spinning disk models, part I: derivations of equations of motion, *Applied Mathematical Modelling* 25 (2001) 541–559.

[18] N. Baddour, J.W. Zu, A revisit of spinning disk models, part II: linear transverse vibrations, *Applied Mathematical Modelling* 25 (2001) 561–578.

[19] W.L. Brogan, *Modern Control Theory*, Prentice-Hall, New Jersey, 1991.

[20] W.H. Press, S.A. Teukolsky, W.T. Vetterling, B.P. Flannery, *Numerical Recipes in Fortran 77*, Cambridge University Press, Cambridge, 2001.